

# Early-A stars from IPHAS, and their distribution in and around the Cyg OB2 association

Janet E. Drew<sup>1,2</sup>, R. Greimel<sup>3,4</sup>, M. J. Irwin<sup>5</sup>, S. E. Sale<sup>1</sup>

<sup>1</sup>*Physics Department, Imperial College London, Exhibition Road, London, SW7 2AZ, U.K.*

<sup>2</sup>*Centre for Astrophysics Research, STRI, University of Hertfordshire, College Lane Campus, Hatfield, AL10 9AB, U.K.*

<sup>3</sup>*Institut für Physik, Karl-Franzens Universität Graz, Universitätsplatz 5, 8010 Graz, Austria*

<sup>4</sup>*Isaac Newton Group of Telescopes, Apartado de correos 321, E-38700 Santa Cruz de la Palma, Tenerife, Spain*

<sup>5</sup>*Institute of Astronomy, Madingley Road, Cambridge CB3 0HA, U.K.*

received, accepted

## ABSTRACT

Stellar photometry derived from the INT/WFC Photometric  $H\alpha$  Survey of the Northern Galactic Plane (IPHAS) can be used to identify large, reliable samples of A0-A5 dwarfs. For every A star, so identified, it is also possible to derive individual reddening and distance estimates, under the assumption that most selected objects are on or near the main sequence, at a mean absolute  $r'$  magnitude of 1.5 – 1.6. This study presents the method for obtaining such samples and shows that the known reddenings and distances to the open clusters NGC 7510 and NGC 7790 are successfully recovered. A sample of over 1000 A stars is then obtained from IPHAS data in the magnitude range  $13.5 < r' < 20$  from the region of sky including the massive northern OB association Cyg OB2. Analysis of these data reveals a concentration of  $\sim 200$  A stars over an area about a degree across, offset mainly to the south of the known 1–3 Myr old OB stars in Cyg OB2: their dereddened  $r'$  magnitudes fall in the range 11.8 to 12.5. These are consistent with a  $\sim 7$  Myr old stellar population at  $DM = 10.8$ , or with an age of  $\sim 5$  Myr at  $DM = 11.2$ . The number of A stars found in this clustering alone is consistent with a lower limit to the cluster mass of  $\sim 10^4 M_\odot$ .

**Key words:** surveys – stars: early-type – stars: distances – open clusters and associations: individual (Cyg OB2, NGC 7510, NGC 7790)

## 1 INTRODUCTION

In the spectra of stars, the  $H\alpha$  line is a prominent marker both as an emission line and as an absorption feature.  $H\alpha$  surveys are generally seen as vehicles for identifying emission line nebulae and stars associated with, primarily, the early and late phases of stellar evolution. In the case of IPHAS, the INT/WFC Photometric  $H\alpha$  Survey of the Northern Galactic Plane (Drew et al. 2005), the quality of the digital photometry in the 3 survey filters,  $r'$ ,  $i'$  and  $H\alpha$ , also allows the strong  $H\alpha$  absorption associated with A-type stars near or on the main sequence to be used as a tool to select these early-type objects easily and reliably. Furthermore, the photometry is sufficient to provide estimates of reddenings and distances. The aim of this paper is to demonstrate how this capability may be exploited. In so doing, we shall verify the method against two test cases, and present an example of this selection at work.

We shall show that the selection of A stars from the IPHAS ( $r' - H\alpha$ ,  $r' - i'$ ) colour-colour plane yields mainly samples of A0-A5 dwarf candidates. These early-type dwarfs

of intermediate mass are expected to remain near the main sequence for not much longer than  $\sim 100$  million years, and so will typically trace relatively young environments – which are a defining feature of the thin disk population of our Galaxy. Objects of this type selected via their maximal  $H\alpha$  absorption have been exploited before as probes of structure within the galactic plane: in a series of papers, S. McCuskey and collaborators identified them in objective prism data down to  $V \sim 12$  and then mapped their distribution (see e.g. McCuskey & Houk 1971, McCuskey & Lee 1976). This technique can be picked up again and applied to the IPHAS database starting from a bright limit of  $\sim 13$ th magnitude, reaching down to  $\sim 20$ th. As IPHAS approaches completion, and its catalogue database is becoming public (Gonzalez-Solares et al. 2008), the targeted selection of A stars can be applied to a range of problems across the northern Galactic plane, ranging from focused studies of individual clusters to tracing large scale Galactic disk structure.

The main application considered here is of the more localised type – to the still enigmatic Cyg OB2 associa-

tion: data from 21 IPHAS fields covering the sky in and around this massive OB association are presented and analysed. Cyg OB2 is the most impressive of the northern hemisphere's Galactic OB associations. Our aim is to use the A-star distribution to better define the extent and nature of this massive cluster. This example also serves to show that even very young regions – 1–3 Myrs old in this case (Hanson 2003) – can be usefully explored by this means.

Cyg OB2 (VI Cygni) is home to the only known northern hemisphere O3 stars (Walborn et al. 2002). It was first recognised for the very massive cluster that it is by Reddish, Lawrence & Pratt (1967), who carried out the first extensive study of the region. They placed it at a distance of 2.1 kpc, based on the apparent magnitude of late B stars. They also defined its extent as a  $29 \text{ pc} \times 17 \text{ pc}$  ellipse centred on RA 20 32 30 Dec +41 30 00 (J2000), and placed its mass in the range  $0.6 - 2.7 \times 10^4 M_{\odot}$ . However now, mainly as the result of the work by Massey & Thompson (1991), the main concentration of OB stars is recognised as lying just to the NE of the VI Cyg No 8 trapezium located at RA 20 33 06 Dec +41 22 30 (J2000), at the nearer distance of 1.7 kpc ( $DM = 11.2$ ). This was not so clearly evident, to begin with, because of the substantial reddening of the main association:  $A_V \sim 6$  is typical for Massey & Thompson's (1991) OB population. On the basis of 2MASS NIR photometry of the region, Knödlseeder (2000) argued that Cyg OB2 could be even more massive than Reddish et al's (1967) estimate, perhaps reaching as much as  $10^5 M_{\odot}$ , and could contain as many as  $2600 \pm 400$  OB stars. This has since been challenged by Hanson (2003), who has also shown that recent recalibrations of OB star absolute magnitudes may require a further reduction of the distance to Cyg OB2 to  $\sim 1.4$  kpc (or  $DM = 10.8$ ).

The paper is organised as follows. The next section presents the main features of IPHAS and the resultant database. Then in Section 3, the IPHAS ( $r' - H\alpha$ ,  $r' - i'$ ) colour-colour plane is discussed from the perspective of the reliable selection of A stars from it, how they may be dereddened, and how this selection maps onto a mean absolute magnitude. We then present two test cases, in the form of the well-studied open clusters NGC 7510 and NGC 7790, to show that the selection works as expected in recovering their known distances and reddenings. This prepares the way for the challenge of exploring the Cyg OB2 region in section 5, in which the full impact of the early A star absolute magnitude sensitivity to age, at the youngest ages, is seen. We conclude with a comment on our findings and on further development and application of the A-star selection technique.

## 2 OBSERVATIONS: IPHAS PHOTOMETRY

A full description of IPHAS data-taking and data-processing has been given by Drew et al. (2005). Here, we mention again only the key features of the observations.

All IPHAS imaging is obtained with the Wide Field Camera (WFC), mounted on the 2.5-metre Isaac Newton Telescope, in La Palma. The WFC is an imager comprising 4 AR-coated, thinned  $4K \times 2K$  EEV CCDs arranged in an L shape, capturing data from an on-sky area of approximately 0.3 of a square degree. With a pixel dimension of  $13.5 \mu\text{m}$ , corresponding on-sky to  $0.333 \times 0.333 \text{ arcsec}^2$ , the

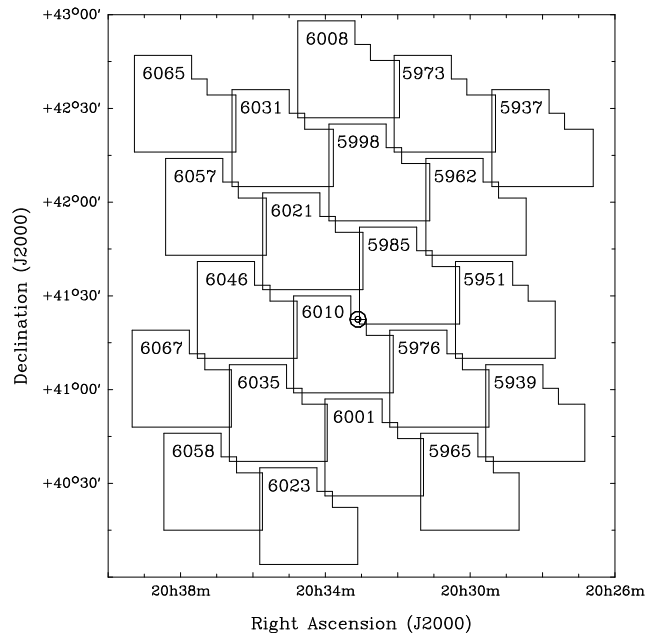


**Figure 1.** The positions of the extracted IPHAS field-pair overlaps in and around CygOB2. The black concentric circles in between fields 5985 and 6010 mark the often-quoted centre of Cyg OB2 (e.g. as in Knödlseeder 2000).

instrument is able to exploit the sub-arcsecond seeing frequently encountered at the telescope site. All the observations of the Cyg OB2 region, presented here, were obtained during the clear moonless nights of 8 and 9 August 2004. The data on the open clusters NGC 7510 and 7790 were obtained on grey nights, in stable conditions, respectively on 26 July and 22 October 2005.

A complete IPHAS observation of any sky position consists of two pointings, the second at an offset of 5 arcmin W and 5 arcmin S with respect to the first. This strategy both enhances the overall photometric quality of the final survey and ensures that stars falling into a gap between the mosaiced CCDs in one exposure are captured in the partner exposure. In this study we only consider point sources that are well-detected in both exposures: this limits the sky extent of the overlap between each field pair to a near-square of side 31 arcmin. Within this there is an irregular grid of inter-CCD gaps, with the result that the sample of point sources discussed here drawn from each field pair comes from a sky area of  $0.22 \text{ deg}^2$ : since there is very little overlap between adjacent field pairs when they are combined in this way, all the Cyg OB2 fields together span close to 90 percent of the total available area of  $\sim 5 \text{ deg}^2$ . The rough sky outlines of the IPHAS field-pair overlaps in the Cyg OB2 region are shown in Fig. 1. The coordinates of the centres of all catalogue extractions discussed in this paper are listed in Table 1, along with other relevant data.

Throughout this paper field pairs are named just by the 4-digit number (column 1 in Table 1) that tags the initial field pointing in the IPHAS database.

At each WFC pointing, imaging is carried out through three filters. These filters are narrow-band  $H\alpha$  (FWHM  $95 \text{ \AA}$ ), Sloan  $r'$  and Sloan  $i'$ . The exposure times in these

**Table 1.** Co-ordinates of field-pair centres, extracted sky areas and object counts.

| IPHAS<br>field<br>number | Extraction Centre Coordinates |               |                          |                       | Extracted area<br>(arcmin $\times$ arcmin) | Star counts: $13.5 \leq r' \leq r'_{\max}$ |                                  |            |
|--------------------------|-------------------------------|---------------|--------------------------|-----------------------|--|--|----------------------------------|------------|
|                          | RA<br>(2000)                  | Dec<br>(2000) | $\ell$<br>( $^{\circ}$ ) | $b$<br>( $^{\circ}$ ) |  | total                                      | candidate A dwarfs<br>(0.02 cut) | (0.03 cut) |
| <hr/>                    |                               |               |                          |                       |  |  |                                  |            |
| NGC 7510                 |                               |               |                          |                       |  |  | $r'_{\max} = 19.0$               |            |
| 7366                     | 23 11 00                      | +60 34 00     | 110.90                   | +0.06                 | 6 $\times$ 6                               | 460  | 34                               | 53         |
| <hr/>                    |                               |               |                          |                       |  |  |                                  |            |
| NGC 7790                 |                               |               |                          |                       |  |  | $r'_{\max} = 19.5$               |            |
| 7626                     | 23 58 24                      | +61 13 00     | 116.60                   | -1.00                 | 6 $\times$ 6                               | 601  | 33                               | 43         |
| 7626                     | 23 58 08                      | +61 24 30     | 116.60                   | -0.81                 | 31 $\times$ 31                             | 8623                                       | 68                               | 140        |
| <hr/>                    |                               |               |                          |                       |  |  |                                  |            |
| Cyg OB2 region           |                               |               |                          |                       |  |  | $r'_{\max} = 20.0$               |            |
| 5937                     | 20 28 00                      | +42 20 30     | 80.48                    | +2.18                 | 31 $\times$ 31                             | 2037                                       | 41                               | 57         |
| 5939                     | 20 28 12                      | +40 52 30     | 79.31                    | +1.30                 | "  | 2362                                       | 60                               | 83         |
| 5951                     | 20 29 01.6                    | +41 25 30     | 79.85                    | +1.49                 | "  | 2363                                       | 107                              | 133        |
| 5962                     | 20 29 50.6                    | +41 58 30     | 80.38                    | +1.69                 | "  | 2472                                       | 43                               | 57         |
| 5965                     | 20 30 00.4                    | +40 30 30     | 79.21                    | +0.81                 | "  | 1448                                       | 49                               | 65         |
| 5973                     | 20 30 42                      | +42 31 30     | 80.92                    | +1.89                 | "  | 2251                                       | 57                               | 80         |
| 5976                     | 20 30 51                      | +41 03 30     | 79.86                    | +0.85                 | "  | 2258                                       | 68                               | 96         |
| 5985                     | 20 31 40.5                    | +41 36 30     | 80.29                    | +1.20                 | "  | 4334                                       | 172                              | 223        |
| 5998                     | 20 32 30.5                    | +42 09 30     | 80.82                    | +1.40                 | "  | 2195                                       | 80                               | 98         |
| 6001                     | 20 32 39                      | +40 41 30     | 79.66                    | +0.51                 | "  | 2067                                       | 46                               | 67         |
| 6008                     | 20 33 21.5                    | +42 42 30     | 81.36                    | +1.60                 | "  | 1716                                       | 19                               | 34         |
| 6010                     | 20 33 30                      | +41 14 30     | 80.19                    | +0.71                 | "  | 2942                                       | 48                               | 77         |
| 6021                     | 20 34 20.7                    | +41 47 30     | 80.73                    | +0.91                 | "  | 2274                                       | 47                               | 70         |
| 6023                     | 20 34 27.5                    | +40 19 30     | 79.57                    | +0.01                 | "  | 1090                                       | 4                                | 8          |
| 6031                     | 20 35 10.8                    | +42 20 30     | 81.26                    | +1.11                 | "  | 1294                                       | 7                                | 9          |
| 6035                     | 20 35 17                      | +40 52 30     | 80.10                    | +0.22                 | "  | 2169                                       | 77                               | 102        |
| 6046                     | 20 36 09.5                    | +41 25 30     | 80.64                    | +0.42                 | "  | 1509                                       | 8                                | 16         |
| 6057                     | 20 37 01.3                    | +41 58 30     | 81.18                    | +0.62                 | "  | 951  | 0                                | 3          |
| 6058                     | 20 37 07.5                    | +40 30 30     | 80.02                    | -0.28                 | "  | 1018                                       | 5                                | 7          |
| 6065                     | 20 37 52.4                    | +42 31 30     | 81.71                    | +0.83                 | "  | 1221                                       | 5                                | 12         |
| 6067                     | 20 37 58                      | +41 03 30     | 80.55                    | -0.08                 | "  | 1151                                       | 8                                | 10         |
| <hr/>                    |                               |               |                          |                       |  |  |                                  |            |
| (Cyg OB2 region totals:) |                               |               |                          |                       |  |  | 910                              | 1250       |
| <hr/>                    |                               |               |                          |                       |  |  |                                  |            |

three filters are 120 sec ( $H\alpha$ ), 30 sec ( $r'$ ) and 10 sec ( $i'$ ). Since it is required that every star considered is imaged in both overlapping pointings, the effective exposure times are twice as long. Every night of IPHAS observing incorporates observations of standard fields, in order to permit photometric calibration in the three observed bands. Presently the  $H\alpha$  narrow-band observations are tied to the  $r'$ -band calibration in the same way as described by Gonzalez-Solares et al. (2008).

A further criterion applied in our selection of candidate A stars is that the CASU pipeline processing and cataloging the data, identifies them as point-like in  $r'$  and  $i'$ , to a high confidence level (i.e. as members of morphology classes -1 and -2, Irwin 1985 and 1997). The photometric error in the resultant catalogue of point sources ranges from entirely negligible at the adopted bright limit (13th magnitude in  $r'$ ), to, typically, 0.03 in  $r'$ , 0.06 in ( $r' - H\alpha$ ) and 0.04 in ( $r' - i'$ ) at the chosen faint limit ( $r' = 20$ ).

### 3 METHOD

#### 3.1 The IPHAS colour-colour plane, illustrated by an example from Cyg OB2

An example of derived colours for a final selection of point sources is shown in Fig. 2. These are the data for IPHAS field

6010, which includes the nominal centre of Cyg OB2. All 2943 stars plotted fall in the magnitude range  $13 \leq r' \leq 20$ . To understand what is implied by this source distribution we make use of the solar-metallicity synthetic tracks that were given in Drew et al. (2005). On Fig. 2 we have superimposed a curve that defines an approximate upper bound on the colour-colour plane location of early A dwarf stars. More precisely this is the reddening line derived using as template the solar metallicity A0V flux-calibrated spectrum from the library due to Pickles (1998), shifted to higher  $r' - H\alpha$  by 0.03. The reddening law used here is a mean Galactic law, with  $R = 3.1$  (Howarth 1983).

The main features of the distribution of stars in the colour-colour plane (Fig. 2) are (i) a foreground unreddened main sequence, beginning at a spectral type of  $\sim G0$  (at  $r' = 13$ ); (ii) an intermediate group of lightly reddened stars ( $A_V \lesssim 3$ ), for which the earliest detected spectral type shifts to  $\sim F0$  (at  $r' \sim 14.5$ ); (iii) a concentration of stars spread between the reddened  $A_V = 4.5$  and  $A_V = 7$  MS lines, and reaching down to and below the early-A dwarf limit line. It can be deduced from the observed magnitudes and colours that the stars in the first two groups will be located at distances of no more than  $\sim 500$  pc. This impression is consistent with a study by McCuskey and Houk (1971) of A stars brighter than  $V = 13$  in which they remarked on a declining stellar density between 500 pc and 1 kpc in this part of the

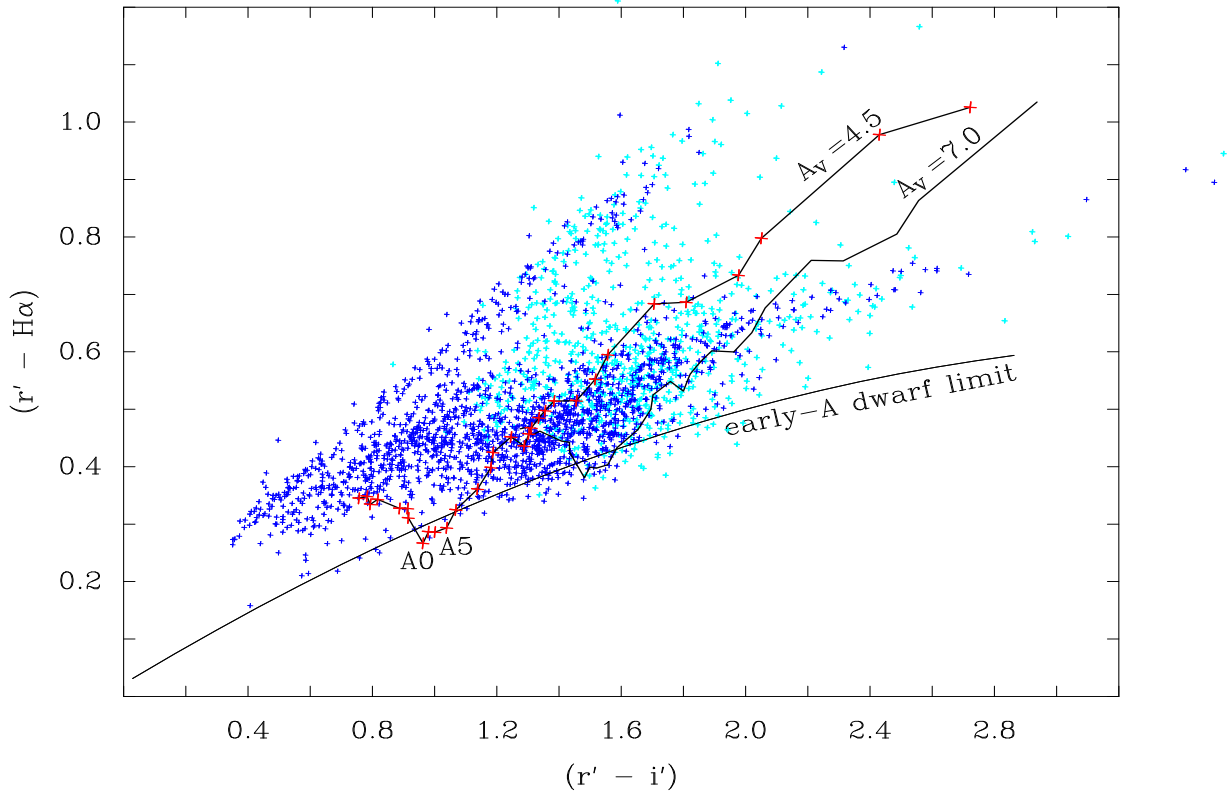


**Figure 2.** The  $(r' - H\alpha, r' - i')$  colour-colour plane of IPHAS field 6010 point sources, selected from the magnitude range  $13 \leq r' \leq 20$ . The black line running along below most of the data points and labelled ‘Early A dwarf limit’ is the reddening line below which the great majority of point sources are expected to be near main sequence A0-A5 stars. Two reddened main sequences constructed from synthetic photometry based on the Pickles (1998) library of flux-calibrated spectra are also drawn (in black also). The red crosses on the  $A_V = 4.5$  sequence pick out the data points that make it up (spanning spectral types O5V to M4V). The IPHAS photometric data are colour-coded according to source  $r'$  magnitude:  $13 \leq r' < 19$ , darker blue;  $19 \leq r' < 20$ , light blue.

Plane, beyond a high concentration found between 200 and 300 pc (see Fig. 7 of their paper). Group (iii) in Fig. 2 is representative of the Cyg OB2 region. Previous work on Cyg OB2 itself have claimed typical reddenings in the range from  $A_V \simeq 4$  to  $\simeq 7$  (Massey & Thompson 1991, Hanson 2003). In Fig. 2 it can be seen that the colour-colour plane is well occupied in this range. It is worthy of note that redward of the  $A_V = 7$  main sequence there is a distinct thinning out of stars. This is mainly attributable to the faint limit imposed on the included data (cf. Fig. 11 discussed in section 5).

### 3.2 The ingredients of IPHAS early-A star selection

At the heart of the method of selection is the choice of a suitable cut along the lower edge of the main stellar locus in the  $(r' - H\alpha, r' - i')$  plane that separates off candidate early-A dwarfs from what will most commonly be later-type stars. Once a group of candidate objects has been picked out in this way, it is straightforward to use the measured  $r' - i'$  of each object to derive its reddening, and then to deredden its measured apparent  $r'$  magnitude. If a suitable averaged absolute magnitude is available, it becomes possible as a next step to determine the distance modulus ( $DM = 5 \log D - 5$ ) for the sample. This enables the construction of a reddening map for the area of sky studied and gives a picture of

how the A stars are distributed with distance. From this approach, one does not expect to derive accurate reddenings and distances for individual candidate A dwarfs, for a number of reasons including that the photometry cannot pin down the A sub-type to within better than 2 to 3 subtypes, and that the absolute magnitude spread at each sub-type is in any case significant (Jaschek & Gomez 1998). What should emerge is a reliable picture in a statistical sense, insofar as the mean properties of the selected population of objects are well-defined.

The shape of the lower edge of the main stellar locus in the  $(r' - H\alpha, r' - i')$  plane will always follow a segment of the reddening curve of an early-A dwarf, as was first noted by Drew et al. (2005). Such a curve is therefore appropriate to use as the cut line. Furthermore, in Fig. 2, it can be seen from the labelling of the  $A_V = 4.5$  main sequence that spectral types A0 to A5 form a line segment running essentially parallel to the reddening line labelled “A dwarf limit” (actually the A0V reddening line shifted upward by  $\Delta(r' - H\alpha) = 0.03$ , in this instance). This is a direct consequence of the fact that the  $H\alpha$  absorption equivalent width reaches a crudely defined maximum of 11 – 13 Å, across this dwarf sub-type range (cf. comment on this in Drew et al. 2005, section 5).

This is not just a quirk of the stars selected by Pickles (1998) that were used as a basis for the synthetic photom-

etry. To confirm this crucial point, the  $H\alpha$  line profiles of near-solar metallicity A dwarfs extracted from the Indo-US spectral library (Valdes et al. 2004) have been compared with those of stars of neighbouring spectral type and luminosity class. The results of this are summed up in simplified form in Fig. 3. The diagram shows that in the mean, A0-5 dwarfs (data on 28 stars combined) are better separated from B9 dwarfs (17 stars), than from A6-A8 dwarfs (7 stars). Given how spectral classification first arose, this is to be expected. The luminosity class comparison is not on such a strong statistical footing, as only 16 giant-star spectra make up the comparison set. Nevertheless, it is clear that the  $H\alpha$  absorption equivalent width in an early-A giant is less, on average, than in an early-A dwarf. On an object by object basis there is enough scatter that the distinction between, especially,  $>A6$  and  $<A5$  dwarfs is not always in the expected sense. At the same time there is some compensation through the empirical fact that the late A near main sequence range is not as well populated with objects as at early A: the bright sample of Abt & Morrell (1995 Table 5) shows that around 1 in 3 luminosity class V and IV stars are A5 or later.

This pattern of behaviour translates into reddening lines in the  $(r' - H\alpha, r' - i')$  plane as shown in Fig. 4. For clarity each reddening line drawn has the A0V reddening line subtracted from it, causing the ordinate in the diagram to become  $\Delta(r' - H\alpha)$ . The A0-A5 V reddening lines, drawn in black, lie below those for adjacent dwarf spectral types and luminosity class III. The appearance of this diagram gives an indication of the  $\Delta(r' - H\alpha)$  range that can be associated exclusively with the early-A dwarfs: it is likely to be  $\sim 0.02$ , with the A0V curve used here defining  $\Delta(r' - H\alpha) = 0.0$ . Photometric error, together with the inevitable gradual mixing in of (mainly) later type dwarfs as the cut line is raised, stands in the way of a fixed recommendation for placing of the cut line. If the aim of selection is to be inclusive of all A dwarfs, choosing a cut at  $\Delta(r' - H\alpha) = 0.04$  or  $0.05$  would make more sense. Hales et al (2008) have obtained spectra of candidates selected using this more generous criterion and find that they are the expected A stars.

Here we explore the effect of gradually raising the cut on the selection process, to see how increased sample size trades against increased likelihood of sample contamination. The fit to the unshifted A0V line in the  $(r' - H\alpha, r' - i')$  plane that we use is a simple quadratic:

$$(r' - H\alpha) = -0.009 + 0.330(r' - i') - 0.0455(r' - i')^2 \quad (1)$$

The other quantitative issues to settle are the median intrinsic  $r' - i'$  colour to associate with A0-A5 dwarfs (needed for dereddening), and the median absolute magnitude,  $M(r')$  that should be adopted for them. To associate absolute visual magnitude with dwarf spectral type and colour, we use the data based on Hipparcos measurements presented by Houk et al. (1997). To find suitable median values, it is necessary to consider how a typical dwarf luminosity function would map onto the A0-A5 range and pick out the expected spectral type and colour of the median absolute magnitude for this spectral type range. To do this, we use the main sequence luminosity function derived by Murray et al. (1997) also from Hipparcos data. Houk et al. (1997) give  $M_V = 0.82$  for A0, and 1.76 for A5 and note

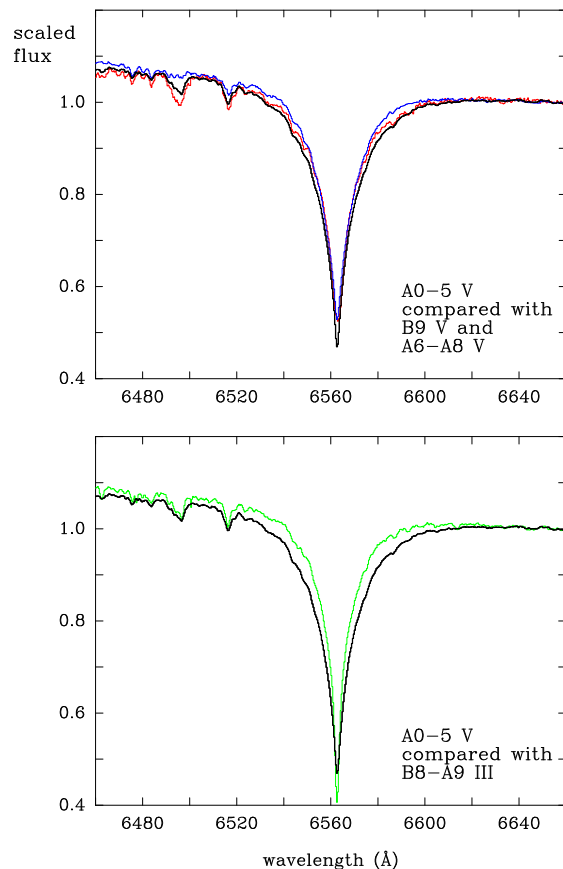


**Figure 3.**  $H\alpha$  line profiles for spectral types of early-A dwarf and adjacent spectral classes. Each profile is the merger of many taken from the Indo-US library of coude spectra (Valdes et al. 2004). The top panel provides a comparison of A0-5 dwarfs (in black) with B9V (blue) and A6-8 (red) dwarfs, while the bottom shows the difference between A0-5 dwarfs and giants (green) at  $\sim A$  type. Before merging, the spectra were rescaled to yield unit flux at 6640 Å, to facilitate the comparison without introducing further corrections that might alter the very subtle depth differences across the central  $\sim 80$  Å of the  $H\alpha$  profile.

a spread of 0.39 mags in absolute magnitude at each spectral sub-type. Based on the data in Murray et al. (1997), a median  $M_V$  of  $\sim 1.5$  is reasonable, for which the intrinsic  $B - V$  is  $\sim 0.1$  (Houk et al. 1997). From the main sequence colours tabulated by Kenyon & Hartmann (1995), intrinsic  $V - R_C \simeq 0.03$ , and  $R_C - I_C \simeq 0.06$  are implied (spectral type A3-4).

This line of reasoning leads to a median intrinsic  $r' - i'$  of 0.06, for which the uncertainty is unlikely to be more than  $\pm 0.02$ . To derive the colour excess due to extinction,  $E(B - V)$ , from an observed value of  $r' - i'$ , this intrinsic colour is subtracted to give  $E(r' - i')$ , which is then multiplied by 1.58. To obtain the visual extinction,  $A_V$ ,  $E(r' - i')$  should be multiplied by 4.91. These transformations apply to the case of  $R = A_V/E(B - V) = 3.1$ , defining the most commonly encountered Galactic extinction law. Where non-standard reddening laws are thought likely to apply (e.g.  $R$  approaching 5 as in sightlines dominated by molecular gas),

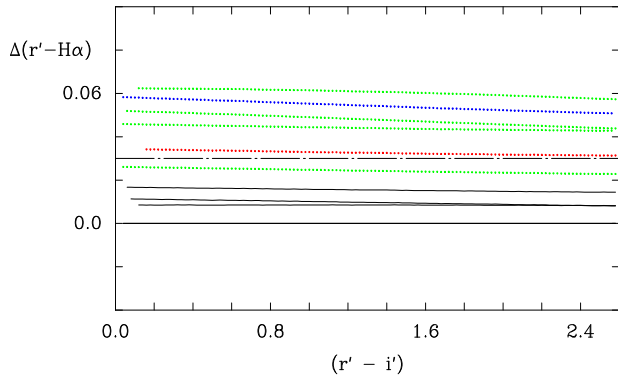


**Figure 4.** Reddening lines derived from the IPHAS colour-colour plane for spectral types in the early-A dwarf range plotted as differences with respect to the A0V reddening line. The same colour code is in use as in Fig. 3, e.g. A0-5 dwarf lines are drawn in black. The fluxed spectra used to synthesise these tracks were taken from the Pickles (1998) library. The lowest line, along the horizontal axis, is the A0V reddening line. Note that  $\Delta(r' - H\alpha) = 0.02$  runs just below the A0 III line, the lowest green line; whereas  $\Delta(r' - H\alpha) = 0.03$ , drawn in as a dash-dotted line, falls just under the A7V line (in red). The blue line is derived from the B9V reddening line.

it would make more sense to refer all reddenings to either the  $r'$  or  $i'$  band, rather than to  $V$  in view of the fact that atypical laws vary away from the norm most strongly in the blue-to-visual part of the optical spectrum (Cardelli, Clayton & Mathis 1989). Specifically, the following relations can be applied:  $A_{r'} = 4.13E(r' - i')$ , and  $A_{i'} = 3.13E(r' - i')$  (using tabulated data from Schlegel, Finkbeiner & Davis 1998). In the cases examined here (sections 4 and 5), previous studies have found the average Galactic extinction law or laws very like it to be satisfactory.

The choice of representative absolute magnitude can be subject to systematic variation, given that the age spread of A dwarfs within 80 pc of the Sun (the samples used by both Houk et al. 1997, and Murray et al. 1997) is not guaranteed to be the same as that in another potential target region. Domingo & Figueras (1999, Fig. 7) have analysed A3-9 main sequence stars drawn from essentially the same Hipparcos sample as that discussed by Houk et al (1997) and show that the earliest among them are indeed quite widely scattered in  $M_V$ , with mean magnitude  $\sim 1.5$ . But they also demonstrate these field stars lie on and smeared above the zero-age main sequence (ZAMS), expected to fall at  $M_V \sim 2$  – that is, these stars may have ages of up to  $\sim 0.5$  Gyr (based on comparison with isochrones due to Schaller et al. 1992). At ages greater than  $\sim 1$  Gyr all stars on or near the early A main sequence will have evolved away.

In Cyg OB2, a region that may be as young as 1–3 million years old (Hanson 2003), we can anticipate that stars with the intrinsic  $(r' - i')$  colours of early-A dwarfs are more massive stars still approaching the ZAMS. Such objects are evolving almost horizontally on the HR diagram and are likely to arrive on the main sequence as mid-late B stars at an age of  $\sim 5$  Myrs (Siess, Dufour & Forestini 2000). Accordingly these are stars with significantly brighter  $M(r')$  than those destined for the early-A ZAMS, after a pre main

**Table 2.** The evolution of  $M(r')$  for stars of early-A ( $r' - i'$ ) with cluster age. These rough figures are derived from the  $Z = 0.02$  theoretical isochrones of Siess et al. (2000). Note that at the youngest ages of  $\sim 3$  Myr or less, there is a greatly increased likelihood that these objects will exhibit circumstellar  $H\alpha$  emission, rather than maximal absorption (i.e. they will not lie along the bottom of the IPHAS main stellar locus).

| age (Myr) | typical $M(r')$ |
|-----------|-----------------|
| 2         | 0.0             |
| 3         | 0.5             |
| 5         | 1.0             |
| 7         | 1.4             |
| 10        | 1.8             |
| 20–100    | 1.9–2.0         |
| 300       | 1.6             |

sequence evolution taking around 10 Myrs or so (Palla & Stahler 1993; Siess et al. 2000).

Because this age effect can be significant, we give in Table 2 some representative values for  $M(r')$  as a function of age that have been derived from the isochrones of Siess et al. (2000). Up to  $\sim 10$  Myrs,  $M(r')$  declines markedly, and then remains close to  $\sim 2$  for a further  $\sim 100$  Myrs or so – at the end of which, evolution away from the main sequence begins. In the absence of any independent constraint on population age or mix, it seems likely that the best guess for the general field in the Galactic disk will be around or slightly fainter than the Hipparcos value of  $M_V \simeq 1.5$ , or  $M(r')$  of  $1.5 - 1.6$ . Since the age-dependence has obvious and serious ramifications for using the selection of early-A dwarfs to analyse Galactic disk sightlines, we begin with two control populations to see how well the method works. Our guinea pigs are the two open clusters, NGC 7510 and NGC 7790, aged 6–10 Myrs (Piskunov et al. 2004) and  $\sim 100$  Myrs (Bragaglia & Tosi 2006), respectively.

Finally, it is worth recalling that binarity will also have some effect on the average absolute magnitude of a population of early A stars. We make no explicit correction for this here beyond favouring  $M(r') = 1.5$ , since we estimate it amounts to a brightening of the mean in the region of 0.1 magnitudes. The following considerations suggest this figure: roughly a half of all stars are binary systems; the mass ratio distribution is not far from flat (Halbwachs et al 2003); hence only in 20–30 % of all binaries is the combined magnitude likely to brighten by more than 0.5 (see figure 1 in Hurley & Tout 1998).

## 4 TEST CASES

### 4.1 Specifics of the extraction of candidate early-A dwarfs

The steps in the extraction are very simple. First,  $r' - H\alpha$  (as a function of  $r' - i'$ ) is used to select stars as candidate early-A dwarfs. Once selected, the measured  $r' - i'$  is converted to a reddening, which then allows the measured  $r'$  to be corrected to a dereddened magnitude.

There is no redundancy in our selection of candidate objects from IPHAS: we use 3 independent quantities to determine 3 properties. Hence it is helpful to bring in e.g.



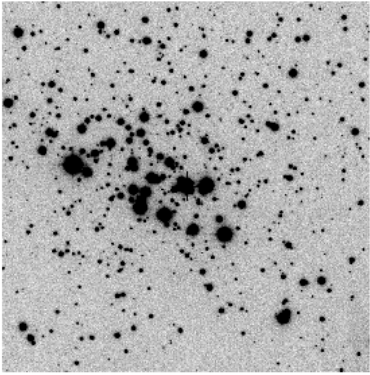


**Figure 5.** The  $6 \times 6$  arcmin<sup>2</sup> field centred on the test cluster NGC 7510, as extracted from the IPHAS database. This is the 30-sec  $r'$  exposures from pointing 7366o. N is up and E to the left.

near-infrared photometry to provide an independent check on the selection. For this, we turn to 2MASS  $J$  magnitudes - where available. Hence, as we select objects below an early-A dwarf limit line, we also collect the 2MASS  $J$  magnitude along with the IPHAS magnitudes and check that the dereddened  $r' - J$  colour falls in the early A-dwarf range (set generously to be  $-0.1 < r' - J < 0.3$  for A0-5V, cf. Kenyon & Hartmann 1995). If the dereddened  $r' - J$  for any object falls outside this range, the object is dropped from consideration. This weeding eliminates between a few percent to 30 percent, depending on the field. If no 2MASS  $J$  magnitude is available or it is an upper limit only, we retain the candidate A-dwarf unverified, rather than throw it away. If we were not to do this, our sample size would be noticeably reduced (by a further factor of up to 20–30% in the worst cases, again depending on the field – it is greater where the reddening is lower).

In all cases, the bright limit is set at  $r' = 13.5$  in order to avoid objects that might be saturated in  $i'$  – particularly in the reddened fields found in the Cyg OB2 region. The faint limit is set at a value appropriate to the sensitivity limit for the IPHAS field under consideration. Whilst exploring this technique of A-dwarf selection, we treat the position of the cut line in the colour-colour diagram as a variable. In particular, we obtain samples of candidates for 4 positions of the cut line: for  $\Delta(r' - H\alpha) = 0.015, 0.02, 0.025$  and  $0.03$ , where  $\Delta(r' - H\alpha)$  is the upward displacement of the A0V reddening line given in equation 1.

#### 4.2 The open cluster NGC 7510

This young open cluster in the northern Galactic Plane has recently been studied by Piskunov et al. (2004), along with a number of southern examples. The aim of this work was to examine the effect of relative youth (main sequence turn-on) on the cluster luminosity function. Piskunov et al. concluded that NGC 7510 is likely to be about 6 million years old. Other authors have favoured ages of  $\sim 10$  million years or more (Sagar & Griffiths 1991, Barbon & Hassan 1996, Kharchenko et al 2005). The CCD photometric study of the cluster by Sagar & Griffiths (1991) earlier found the distance modulus to be  $12.5 \pm 0.3$  and that  $E(B - V)$  ranges from 1.0

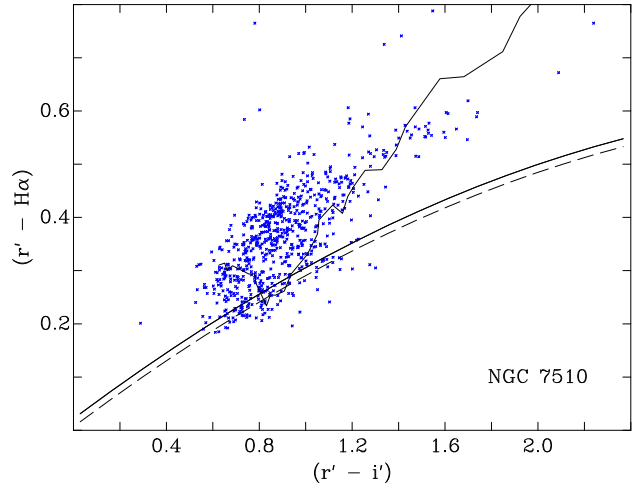


**Figure 6.** The  $(r' - H\alpha, r' - i')$  colour-colour plane of the  $6 \times 6$  arcmin<sup>2</sup> field centred on the young open cluster NGC 7510 (in IPHAS fields 7366/o). The point sources plotted are selected from the magnitude range  $13.5 \leq r' \leq 19.0$ . The parallel solid and dashed lines are the early-A dwarf cut line shifted upward from the A0V reddening line by, respectively, 0.03 and 0.015. The piecewise connected line is the  $E(B - V) = 1.2$  main sequence constructed from synthetic photometry based on the Pickles (1998) library of flux-calibrated spectra.

to 1.3, in good agreement with e.g. Lynga’s (1988) cluster catalogue.

Our selection of candidate A dwarfs is taken from a  $6 \times 6$  arcmin<sup>2</sup> region of sky centred on the cluster (Fig. 5). The faint limit to the selection is set at  $r' = 19$  – two magnitudes above the pipeline estimate of the magnitude limit for the observations of IPHAS fields 7366/o in which NGC 7510 is located. The lowest and highest cut lines applied to the data are shown in Fig. 6, superposed on the colour-colour diagram for NGC 7510 and environs obtained from the IPHAS database.

The results of the selection are shown in Fig. 7. In the upper panel, the raw histogram of star numbers per  $\Delta DM_{1.5} = 0.25$  bin is presented. The distance modulus used here is derived applying a cluster age-appropriate value for  $M(r')$  of 1.5 (see Table 2). The extracted sample sizes are 31, 34, 43 and 53 objects, in order of increasing  $\Delta(r' - H\alpha)$ . In the middle panel, an arbitrarily-scaled quantity directly proportional to the space density of candidate A-dwarfs,  $\rho_A$ , is plotted against  $DM_{1.5}$ . To arrive at  $\rho_A$ , the number of candidate A-dwarfs per distance modulus bin is divided by the cube of the bin mid distance: this corrects for the growing volume associated with each successive histogram bin. The bottom panel shows the relationship between  $DM_{1.5}$  and reddening for two samplings of the data.

The main cluster is very clear, in all three panels of Fig. 7. In the histogram (upper panel), only 5 out of the sample of 34 stars for  $\Delta(r' - H\alpha) = 0.02$  (blue line and points) fall outside the main peak, centred on  $DM_{1.5} = 12.53 \pm 0.04$  (measured by fitting a single Gaussian to the peak). For the largest sample, obtained with  $\Delta(r' - H\alpha) = 0.03$ , 12 stars out of 53 stray away from the cluster peak (green line and points), that itself has shifted downwards slightly to  $DM_{1.5} = 12.48 \pm 0.02$ . The increased proportion of outliers

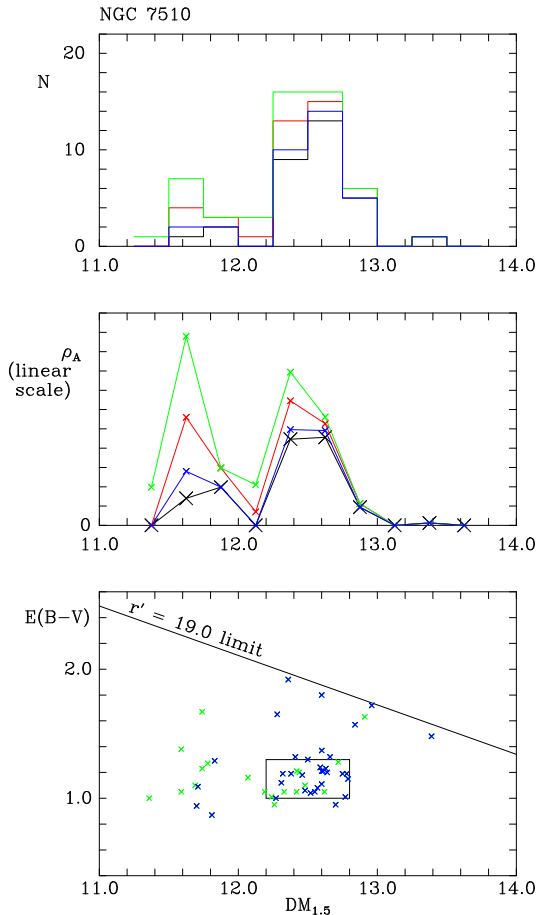


**Figure 7.** The test case of the open cluster NGC 7510. The upper panel shows the distribution of derived distance moduli ( $DM_{1.5} \equiv$  dereddened  $r'$  magnitudes less an adopted median absolute magnitude of 1.5). The four curves shown are for four choices of positioning of the early-A dwarf limit line:  $\Delta(r' - H\alpha) = 0.015, 0.02, 0.025$  and  $0.03$  are respectively in black, blue, red and green. Note that as the limit line is raised, in  $\Delta(r' - H\alpha) = 0.005$  steps, the distribution is better populated but also begins to shift slightly toward lower mean distance modulus. The middle panel is a conversion of the upper panel to an A-star space density distribution, obtained by taking the number of stars in each histogram bin plot, and dividing by cube of the distance. The lower panel shows derived  $E(B-V)$  versus  $DM_{1.5}$ , plotting first the largest sample obtained for the highest position of the cut line ( $\Delta(r' - H\alpha) = 0.03$ , in green), and then overplotting in blue the smaller sample obtained with the cut line lowered to  $\Delta(r' - H\alpha) = 0.02$ . The box, centred on  $DM = 12.5$  and  $E(B-V) = 1.15$ , is the result for NGC 7510 due to Sagar & Griffiths (1991).

hints that sample contamination may indeed be greater, but their impact is small. Another property that does not change very much, as the cut line is raised, is the FWHM of the cluster peak: it remains close to  $\Delta DM = 0.4$  in all 4 cases explored.

As well as being clearly defined, the cluster is also at a mean  $DM_{1.5}$  and typical reddening that is in very good agreement with the results of Sagar & Griffiths (1991). The box superimposed on the reddening plot (bottom panel of Fig. 7) encloses the reddening range they found, and the error bound on the distance modulus:  $1.1 < E(B-V) <$

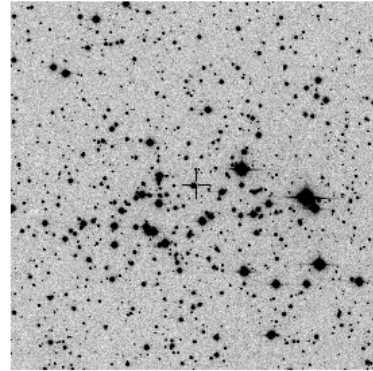


**Figure 8.** The  $6 \times 6$  arcmin<sup>2</sup> field centred on the test cluster NGC 7790, as extracted from the IPHAS database. This is the 30-sec  $r'$  exposures from pointing 7626o. N is up and E to the left.

1.3 and  $DM = 12.5 \pm 0.3$ . The extinction properties of the candidate A dwarfs reveal that there are objects – within the cluster as far as we can tell – at markedly higher extinctions ( $E(B-V) > 1.5$ ) than found in prior optical studies.

The outlier grouping at  $DM_{1.5} \simeq 11.7$  that becomes more evident as the cut line is raised, appear to be as reddened as most of the main cluster group. This similarity favours viewing these outliers as intrinsically brighter objects of similar optical colour within the cluster, rather than as members of an independent foreground cluster. Indeed Piskunov et al. (2004) noticed that there was a case for a younger  $\sim 2$  Myr-old population in NGC 7510 in addition to the dominant 6–10 Myr old component: the A dwarfs in such a component would be nearly 1 magnitude brighter as is implied here (e.g. the  $M(r')$  difference between 3 Myr old and 7 Myr old A stars is given in Table 2 as 0.9 mags). So we see that this selection technique begins to pick up on both generations of stars in NGC 7510.

The middle panel of Fig. 7, corrected to trace A-star space density seemingly brings out this bimodal character even more. However this more physical presentation of the data comes at a price: the correction to space density greatly amplifies both the count and the Poissonian error at lower  $DM$  with respect to those at higher. For example for the data for  $\Delta(r' - H\alpha) = 0.03$  (coloured green), the error on the density peak in the range  $11.5 < DM_{1.5} < 11.75$  is nearly 40 % (just 7 stars), while it is under 20% in the range  $12.25 < DM_{1.5} < 12.75$  (31 stars). This needs to be borne in mind in the later discussion of results for Cyg OB2.

### 4.3 NGC 7790

The open cluster, NGC 7790, is believed to be about 100–120 Myrs old (Bragaglia & Tosi 2006; Gupta et al. 2000) and hence close to the age at which A stars would begin leaving the main sequence. We have extracted the photometry from a  $6 \times 6$  arcmin<sup>2</sup> field centred at RA 23 58.4, Dec +61 13 (J2000, see Fig. 8) and have selected candidate A stars following exactly the same method as for NGC 7510. Given the age of this cluster there is some room to question whether a more firmly main-sequence, slightly fainter absolute magnitude,  $M(r') \simeq 1.9$ , would work better than the



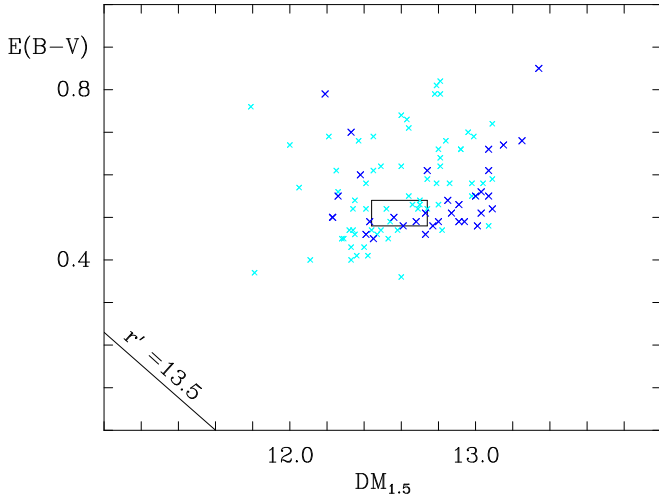


**Figure 9.** Result for the open cluster NGC 7790. Derived  $E(B - V)$  and  $DM_{1.5}$ , are plotted against each other. The larger sample shown in a lighter cyan colour was obtained from the  $31 \times 31$  arcmin<sup>2</sup> overlap of IPHAS fields 7626/o, including NGC 7790. The data shown in blue were obtained from the smaller  $6 \times 6$  arcmin<sup>2</sup> field centred on the cluster. The cut line in both cases was set at  $\Delta(r' - H\alpha) = 0.025$ . The box, centred on  $DM = 12.59$  and  $E(B - V) = 0.51$ , is the result for this cluster due to Gupta et al. (2000).

value of 1.5 more typical of the general field. Staying with  $M(r') = 1.5$ , we arrive at the result shown in Fig. 9 as the blue datapoints. The comparison is made in this case with the results of the photometric study by Gupta et al. (2000): they obtained  $E(B - V) = 0.51 \pm 0.03$ ,  $DM = 12.59 \pm 0.15$ .

Once again, it is clear this method of A-star selection has found a group of objects belonging to the target cluster at a range of reddenings compatible with the results of detailed photometric study. Had we adopted the fainter main sequence absolute magnitude the distribution of stars in Fig. 9 would still have overlapped the Gupta et al distance, but most of the A stars would have been lying at lower  $DM$ . That the brighter field absolute magnitude does a little better suggests that some stars have begun to evolve away from the main sequence.

A second extraction across a larger field of  $31$  arcmin<sup>2</sup>, more than doubles the sample size and mildly smears the appearance of the  $E(B - V)$  versus  $DM_{1.5}$  diagram (the cyan data points in Fig. 9. But contamination of the sample by the general field appears slight. This outcome may imply that A-star selection can become a useful tool for identifying new clusters with economy of effort. This is the main way in which we use it below in the discussion of Cyg OB2.

## 5 CYG OB2

### 5.1 Early-A stars around the centre of Cyg OB2

We now come on to the second main aim of this study: to access a lower stellar mass range than has hitherto been open to examination in Cyg OB2 and its environment. The reward for doing this will be, at minimum, a better picture of the angular extent of this association.

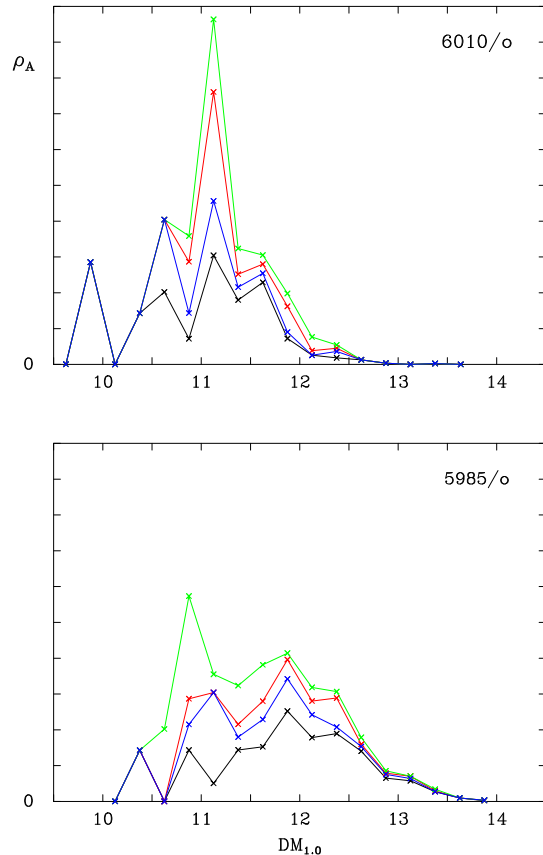


**Figure 10.** The sampled variation of  $\rho_A$  versus provisional distance modulus ( $DM_{1.0} \equiv$  dereddened  $r'$  magnitudes less an adopted median absolute magnitude of 1.0) for fields 6010 and 5985 to either side of the centre of Cyg OB2. In each panel the four curves shown are for  $\Delta(r' - H\alpha) = 0.015, 0.02, 0.025$  and  $0.03$ , and are again respectively black, blue, red and green, as in Fig. 7. The adopted bin size is  $\Delta(DM) = 0.25$ .

We first consider the selection and dereddening of candidate early-A dwarfs in IPHAS fields 6010 and 5985, that straddle the centre of Cyg OB2 (Fig. 1). The colour-colour plane for field overlap 6010 was shown as Fig. 2, from which it was noted that Cyg OB2 is apparent as an excess of objects in the approximate reddening range  $4.5 < A_V < 7$ . As in Fig. 2, no selected object will be fainter than  $r' = 20$ . As for NGC 7510 and NGC 7790, this cut-off magnitude is 2 magnitudes brighter than the reduction pipeline estimate of the magnitude limit of the observations. In this and all other respects, the method of selection is the same as those applied to these test-case clusters.

In Fig. 10, we present the space density distributions for provisional distance moduli,  $DM_{1.0}$ , obtained from early-A dwarf candidates for different offsets of the IPHAS limit line for both fields: as the offset is increased, so the sample size increases. We choose  $M(r') = 1.0$  for now, noting that this corresponds to an age in the region of 5 Myr. In its lowest position the cut line is placed at  $\Delta(r' - H\alpha) = 0.015$  above the A0V reddening line. The increasing contamination with increasing offset potentially brings in intrinsically redder, and fainter, stars, that might bias the derived distribution toward over-estimated reddenings and underestimated dis-

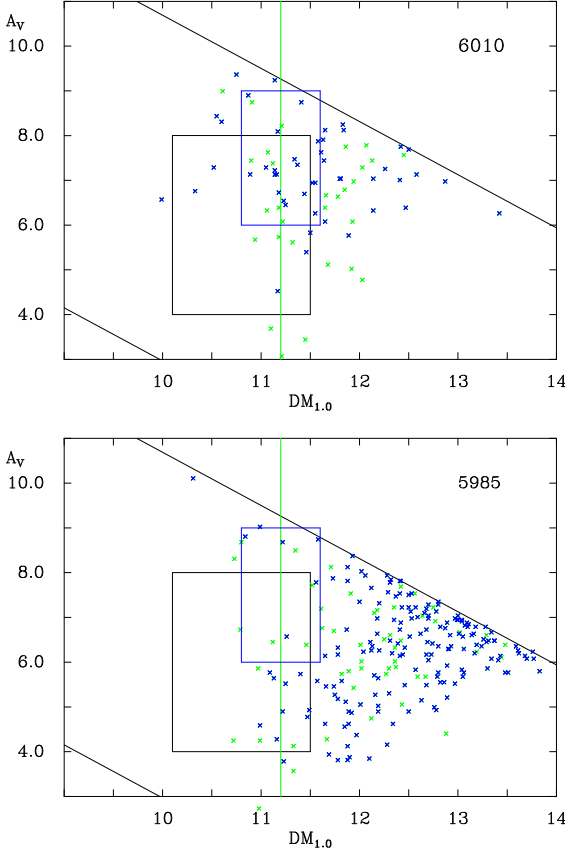


**Figure 11.** Visual extinctions versus provisional distance moduli  $DM_{1.0}$  for fields 6010 and 5985 straddling the centre of Cyg OB2. The dark blue points correspond to objects selected below the  $\Delta(r' - H\alpha) = 0.02$  cut line (cf Fig. 10), while the lighter green points are the objects added to the sample for the highest cut line ( $\Delta(r' - H\alpha) = 0.03$ ). The box drawn in black and the green line are discussed in the text. The box in blue delineates a range in  $DM_{1.0}$  also picked out in Figs 13 and 14.

tance moduli. A very small effect, possibly due to this, may be apparent in the populous, less reddened field (5985) to the NW of the nominal Cyg OB2 centre – while the overall sample size grows from 142 objects (black curve) to 223 (green curve). In field 6010 the shift is negligible and perhaps just positive, while the sample size increases from 37 objects (black curve) to 77 (green curve). To limit Poissonian noise, we will prefer the largest samples obtained on setting  $\Delta(r' - H\alpha) = 0.03$ .

The striking feature of Fig. 10 is the large difference in the A-star density distributions contained in the two neighbouring fields. For 6010, the peak in the range  $11.0 < DM_{1.0} < 11.25$  sits at 3-sigma contrast with respect to the less well-populated bins to either side of it. No such peak is apparent in 5985 and the overall population seems less dense and more distant. To better understand the origin of this, we show in Fig. 11, the relationship between reddening ( $A_V$ ) and  $DM_{1.0}$  in both cases. In field 6010 just to the SE of the nominal centre of Cyg OB2, it is evident that the stars making up the peak population around  $DM_{1.0} \simeq 11$  are seen through visual extinctions of 5 to 8 magnitudes. This contrasts with 5985 where the most common reddening to

$DM_{1.0} \sim 11$  is 4 to 6 magnitudes. The other clear point of contrast is that it is the slower rise of reddening with distance within 5985/o that allows us sight, in this field, of so very many candidate A dwarfs at  $DM_{1.0} > 12$ . We are seeing these objects through a relative reddening hole that has been known about since the work of Reddish et al. (1967, see also Dickel & Wendker 1978, Knödlseider 2000). It is also evident (from Fig. 11), that the  $r' = 20$  magnitude limit applied slices through this more distant population.

The box drawn in black in both panels of Fig. 11 spans the range in distance modulus and extinction obtained by Hanson (2003) in her study of brighter OB stars. The mean  $DM$  she favoured was 10.8. The vertical green line in both panels marks  $DM = 11.2$ , obtained by Massey & Thompson (1991). The tidy picture seen in the case of NGC 7510, a relatively isolated young cluster, is not repeated here. In the upper panel, for 6010, the Hanson (2003) box looks to be displaced to lower distance moduli than the selected A-dwarfs: to bring the two into alignment it would be necessary to increase the assumed A-dwarf absolute magnitude by  $\sim 0.7$ . The Massey & Thompson (1991) distance fares rather better in that the offset is only about 0.3 magnitudes. With either of these comparisons there is a problem in that increasing the adopted absolute magnitude amounts to raising the age of the population, when existing estimates for the age of Cyg OB2 are less than 5 Myr.

In 5985 (lower panel of Fig. 11), the Hanson (2003) Cyg OB2 distance and reddening range exhibits even less connection with the apparent distribution of candidate early-A stars. Much of the early-A population in this field is unlikely to belong to any cluster at a distance below  $\sim 2$  kpc ( $DM_{1.0} \sim 11.5$ ). Indeed, there may be a steady rise in reddening with increasing distance modulus in this field, with little imprint of Cyg OB2 itself.

## 5.2 Candidate A dwarfs across the wider Cyg OB2 region

The larger picture in this region is shown in Fig. 12. Distributions are only shown for fields in which there are more than 50 candidate early-A dwarfs (for  $\Delta(r' - H\alpha) = 0.03$ ). The number of candidate objects per field was given in Table 1. The better populated fields lie mainly in the centre and west of the region studied. The outstanding feature of the A-star density profiles as a function of  $DM_{1.0}$ , apparent from Fig. 12, is the repeated density peak in the  $11.0 < DM_{1.0} < 11.25$  bin in the southern fields (6010, 5976, 6035, 6001 and 5985). High densities at similar distance moduli are also apparent in 5951 and 5998 – but not in the two fields immediately to the north of the nominal Cyg OB2 centre, 6021 and 5985.

To show in greater detail what this may mean, we plot reddening against  $DM_{1.0}$  for fields 6001 and 5976 in Fig. 13. The blue box is drawn around the main concentration of candidate early-A dwarfs found here ( $10.8 < DM_{1.0} < 11.6$ ). Objects in this range make up the overwhelmingly dominant  $\rho_A$  peak seen in Fig. 12 for field 6001 (39 stars, but note that the  $\rho_A$  peak closer to  $DM_{1.0} \sim 10$  is created by just 5 stars and so is much less significant). The reddening in these fields is somewhat higher than in the central part of Cyg OB2 (6010) to the north: for most stars here,  $A_V > 6$ . In field 5976 there is a tail of detected objects to much greater

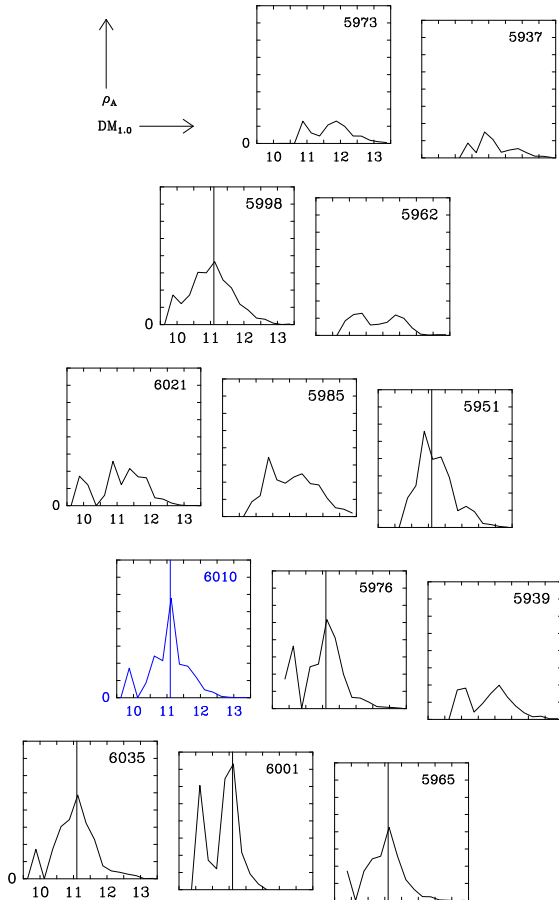


**Figure 12.** Derived candidate early-A dwarf densities as a function of  $DM_{1,0}$  for fields in and around Cyg OB2. The relative positioning of the histograms roughly mimics their on-sky positioning, as shown in Fig. 1. Hence, roughly speaking, N is up and E to the left. To increase the sample sizes, the cut line in the IPHAS ( $r' - H\alpha, r' - i'$ ) plane has been set at maximum ( $\Delta(r' - H\alpha) = 0.03$ ). The most nearly central field, 6010, is picked out in blue. Overlap fields listed in Table 1 with fewer than 50 candidate early-A dwarfs are not shown. In every panel, the axis ranges are the same and, in some, a vertical line is drawn at  $DM_{1,0} = 11.1$ .

distances ( $DM_{1,0} > 12$ ) which is absent from 6001, suggesting that the typical extinction affecting sightlines in 5976 is less severe. This also raises the possibility that the greater obscuration in field 6001 induces more sample incompleteness: undercounting of A stars in this field at  $DM_{1,0} \gtrsim 11.0$  may be more significant.

Finally, we take a look at 0.5–1 degree N and NW of the centre of Cyg OB2, at fields 5998 and 5962 (Fig. 14). Field 5998/o is rather similar to 6010, and fields further south. The character of 5962 is quite different: there is not a concentration of stars in the  $DM_{1,0}$  range, 11.0 – 11.5, and the overall number of candidate A dwarfs is relatively low. The modest pile up at  $A_V \sim 8$  at distance moduli 12.0 to 13.0 in 5962 (Fig. 14) suggests there may be more undiscovered at still higher reddenings, fainter than the imposed  $r' = 20$  limit. Inspection of similar reddening plots (not shown) for the fields neighbouring 5962 supports the impression that

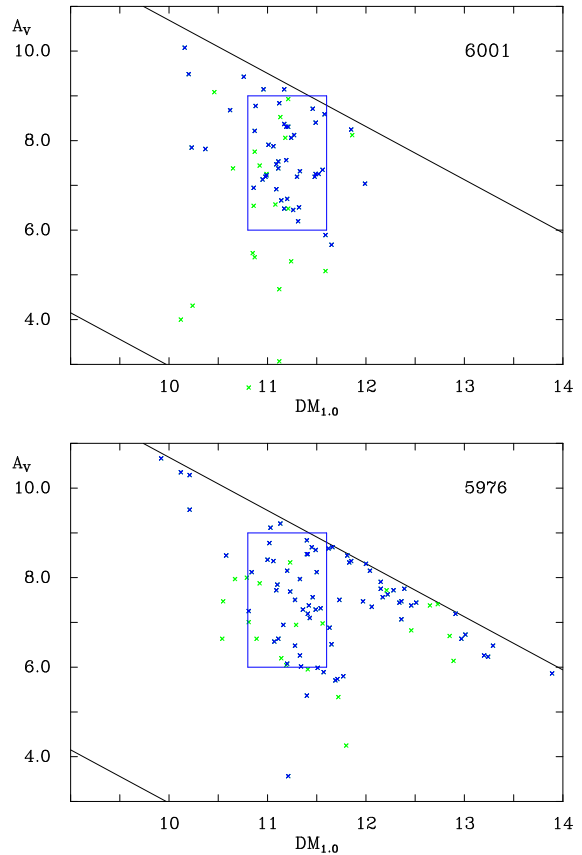


**Figure 13.** Visual extinctions versus provisional distance moduli  $DM_{1,0}$  for fields 6001 and 5976 to the south-west of the centre of Cyg OB2. The dark blue points correspond to objects selected below the  $\Delta(r' - H\alpha) = 0.02$  cut line (cf Fig. 10), while the lighter green points are the objects added to the sample for the highest cut line ( $\Delta(r' - H\alpha) = 0.03$ ). The  $DM_{1,0}$  range picked out by the same blue box in each panel is the peak density region apparent from Fig. 12. To ease comparison, this region is also identified in both Figs. 11 and 14.

incompleteness of this kind is much more of an issue in the extreme north of the region.

### 5.3 Implications for the extent and nature of Cyg OB2

The main implication of Fig. 12 is the clear A-star density peak centred on  $11.0 < DM_{1,0} < 11.25$  in the southern fields, that is most pronounced in field 6001. Is this the real Cyg OB2? This can be looked at in a different way by mapping the positions of the stars with dereddened  $r'$  magnitudes falling in the range  $11.75 < r'_0 < 12.5$  that contribute to this apparent ‘clustering’ (Fig. 15).

On the basis of 2MASS data, Knödlseeder (2000) demonstrated a peak in stellar density at NIR wavelengths that coincides with the heart of Cyg OB2 itself. This region is enclosed by the the red box drawn in Fig. 15. There is not a matching peak in the concentration of A stars here: the IPHAS field pair 6010 does not stand out in this way. Moreover, there is a relatively empty region cutting across the NE corner of 6010, continuing through the south of adjacent

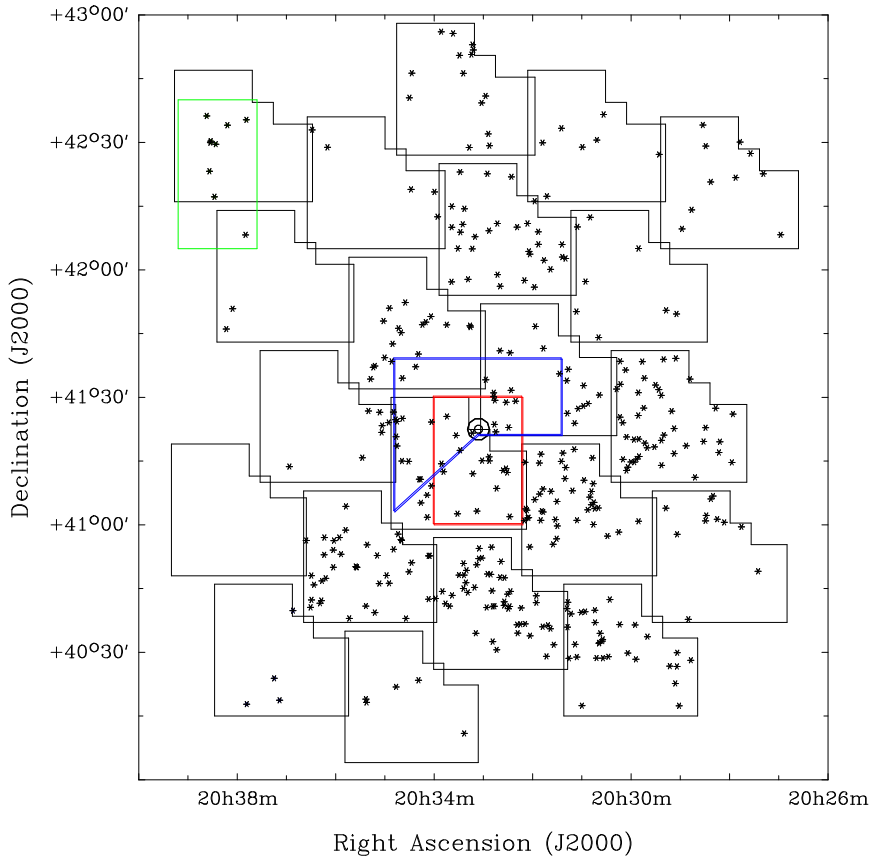


**Figure 15.** The spatial distribution of candidate A dwarfs in the vicinity of Cyg OB2, with dereddened  $r'$  magnitudes in the range  $11.75 \leq r'_0 \leq 12.5$ . The area bounded by the red line roughly matches the area of peak NIR stellar density as identified by Knödlseider (2000). The area bound by the blue line picks out the main concentration of optically identified OB stars (Massey & Thompson 1991). In the NE the green box encloses the stellar population associated with DR 21 discussed by Kumar et al. (2007).

fields 6021 and 5985. This underpopulated region is much the same as that occupied by the OB stars picked out in Massey & Thompson’s (1991) optical study (the rough outline to this region is picked out in blue in Fig. 15, see also Fig. 4 of Hanson 2003). Inspection of the original IPHAS imaging confirms that this anti-correlation is not due to the OB stars creating a bright background swamping the fainter A stars.

As shown in Fig. 15 the east of the region is even more striking for the lack of candidate A dwarfs. This absence was already foretold by the data in Table 1, showing that there are few ordinary A stars to be had at any distance modulus. The appearance of a few in the extreme north-east, in the vicinity of DR 21 (marked in green), may signal the emergence of the new generation of stars linked to this well-known HII region. The median  $r'_0$  for the group is 12.33. If indeed they are as young (1–3 Myrs) as the population of objects analysed by Kumar et al. (2007), they would be 2.9 kpc away (adopting  $M(r') = 0$ ) – the distance also favoured by Kumar et al. (2007).

The major concentration of A dwarf candidates in Fig. 15 is in the southern fields that also stood out in Fig. 12, albeit with a zone of avoidance in the south west (lower part of 5976, extending to most of 5939 further west). If the central field, 6010, is included with these fields (5951, 5965,

5976, 6001, 6035), the total number of plotted objects is 239 – an average of 40 per field. 6001 is the most populous with 49 stars, 6010 the least with 32. This leaves just 125 objects to be shared among the remaining 14 fields in this magnitude range. In broad brush terms, we have roughly 200 A stars spread across an area about 1 degree across, distributed around RA 20h 32m and Dec +41 00 (2000).

The typical dereddened magnitude for this grouping is  $r'_0 \simeq 12.1$ . To be sure of the distance to this structure, an age must be known. The assumption made for Fig. 12 was consistent with an age of 5 Myr, and placed this clustering at distance of 1.7 kpc ( $DM_{1.0} \simeq 11.1$ ). If the typical age can be allowed to be as low as 2 Myr, then  $M(r')$  is required to be as bright as 0.0, driving the distance up to an improbable 2.6 kpc ( $DM_{0.0} = 12.1$ ). A further argument against this solution is that we are seeing evidence here that such young A star populations tend to be sparse – as illustrated by the low counts linked to both DR 21 in the NE and to the main central concentration of optically-detected OB stars – both likely to be only 1–3 Myrs old. It is more plausible to consider ages greater than 5 Myrs, rather than less. For example, an age of  $\sim 7$  Myrs imposes  $M(r') = 1.4$  (Table 2) which then points to a distance modulus close to the value of 10.8, equivalent to a distance of 1.4 kpc, that was favoured by Hanson 2003 based on revised OB-star calibrations.

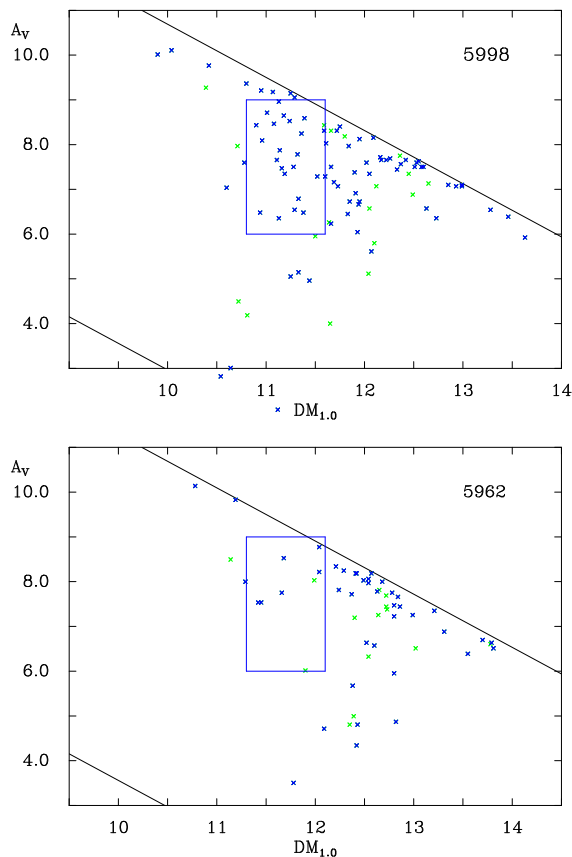


**Figure 14.** Visual extinctions versus provisional distance moduli  $DM_{1,0}$  for fields 5998 and 5962 to the north and north-west of the centre of Cyg OB2. The colours have the same significance as in Figs. 11 and 13.

Accepting an age spread in and around Cyg OB2 seems the best option. If there are very young A-type objects embedded among the OB stars, they are few in number and/or escaping selection by virtue of either modest  $H\alpha$  emission or high extinction ( $A_V > 10$ ). The larger numbers of A stars to the south of Cyg OB2 centre give away the presence of the larger, somewhat older, main cluster. In effect Cyg OB2 can be seen as a further example of cluster ‘rejuvenation’, but on a much grander scale than that already noted in the test case of NGC 7510. What is unclear at the moment is whether the rejuvenation is on the NE periphery of the main cluster, or whether it is more centrally located within a cluster that extends as far north as field 5998, which also exhibits an A-star density peak in the appropriate dereddened magnitude range (Fig. 12). The less elegant solution at this point is to view the swathe of A stars to the south of the nominal centre of Cyg OB2 as evidence of a distinct cluster, of unknown age and distance, unconnected with the known OB stars.

If we can associate  $\sim 200$  A0-A5 near main sequence stars with a 5-7 Myr old southerly cluster, then the combination of Siess et al. (2000) isochrones for this age range and the Kroupa (2001) flattening of the Salpeter IMF below  $0.5 M_\odot$  would imply a total cluster mass in the region of  $10,000 M_\odot$ , and an OB star count of around 200. There are a number of respects in which this estimate is surely on

the low side. First, a minor point is that the sky coverage is only 90 percent. But more important is the fact that the selection of A stars applied here has been fairly conservative in order to keep sample contamination minimal: had the cut line been raised to  $\Delta(r' - H\alpha) = 0.05$ , the number of candidate A dwarfs in the region would nearly double. There is also clear evidence of sample incompleteness due to high and patchy reddening – a problem that appears more marked in the more southerly fields 6001 and 5976 with higher  $\rho_A$  than near the OB star concentration. And finally, this accounting does not include the immediate environs of the OB stars in which fewer stars of early-A colour have yet appeared: applying the same approach as above for a star count of  $\sim 30$  (for e.g. field 6010) at the much younger age of  $\sim 2$  Myrs adds a further  $\sim 10,000 M_\odot$ . A final proper accounting of the total mass in the region of 30,000 to 40,000  $M_\odot$  would not be surprising.

The reputation of Cyg OB2 as the outstanding visible northern OB association remains untarnished. However, the upper limit of the claim by Knödlseider (2000) is difficult to sustain: if this region truly is home to over 2000 OB stars then this appraisal of the A star content has under-counted by an order of magnitude. At least in the core region of Cyg OB2 where the reddening is less severe, so large a discrepancy is unlikely.

## 6 CLOSING REMARKS

This study has had two goals. The first of these was to show how the IPHAS ( $r' - H\alpha, r' - i'$ ) plane may be exploited in a very simple way to yield reliable samples of near main-sequence A0-A5 stars. Such objects in the general field, selected as described here and validated by HIPPARCOS data, will present themselves with a typical absolute magnitude  $M(r')$  of 1.5 – 1.6. Fortunately, for stellar ages of  $\sim 10$  Myrs or more there is little change in this absolute magnitude. For simple single-aged populations a magnitude spread of  $FWHM \sim 0.5$  is to be expected. Demonstrations of this selection at work have been provided by the examples of the open clusters NGC 7510 and NGC 7790.

The second aim has been to apply this A-star selection technique to the challenging example of Cyg OB2. This spectacular northern cluster, immersed in the Cygnus X region of the Galactic Plane, continues to be debated in the literature on account of its uncertain dimensions and distance. The new capability directly bestowed by IPHAS photometry (unsupported, thus far, by spectroscopy) is that of identifying the on-sky distribution of and reddenings of over 1000 A0-A5 stars towards, around, within, and beyond Cyg OB2. The result of this is a clear peak in A-star density, comprising  $\sim 200$  objects, roughly centred on RA 20h 32m and Dec +41 00 (2000), some 20 arcmin south of the VI Cyg No.8 trapezium normally taken as the centre of Cyg OB2.

The most parsimonious interpretation of the results obtained is to treat the southern clustering of A stars and the already known OB star concentration as part of the same cluster, compatible with a distance of 1.4 kpc ( $DM \simeq 10.8$ , Hanson 2003) if the A stars are  $\sim 7$  Myr old, or with 1.7 kpc ( $DM = 11.2$ , Massey & Thompson 1991) if their typical age is  $\sim 5$  Myr. Either solution requires some age contrast between the A stars (5-7 Myrs old) and the main group of



OB stars (1–3 Myrs old, Hanson 2003). This may amount to two main bursts of star formation, or to an indication of a substantial age spread (cf. the case of the ONC cluster discussed by Palla et al. 2005). The presence of a range of ages may help to explain why Cyg OB2 is not associated with bright H II emission despite its very evident rich O star population. The massive cluster, R 136 in the Large Magellanic Cloud exhibits similar behaviour in that its intermediate mass stars appear to be  $\sim 6$  Myrs old, as compared with 1–2 Myrs for the most massive stars (see Massey 2003). Indeed, in Cyg OB2 itself, signs of non-coeval star formation have been noticed before (Massey & Thompson 1991, Hanson 2003). The mass linked to the newly-found A stars in the cluster is at least  $10,000 M_{\odot}$ . As a cautionary note, we point out that it remains possible (if less attractive, see Schneider et al 2006) that the main A-star clustering is at a different distance from the OB stars.

There are two wider applications of this new technique for selecting A stars from IPHAS. First, it is a new tool for use in exploring the structure of the Galactic thin disk. This will be especially incisive when applied to the less reddened outer Galaxy. We have not discussed metallicity here, but it should not create much difficulty: on the one hand, the weak line-blanketing at red wavelengths implies that the  $r' - i'$  colour of A stars will not be metallicity-sensitive, and, on the other, the evidence to date is that metallicities ( $[Fe/H]$ ) in the thin disk at large Galactic radii are not greatly subsolar (e.g. Carraro et al 2007, who find a mean  $[Fe/H]$  of  $\sim -0.35$  for  $R_G$  between 12 and 21 kpc). Second, A-star selection over large sky areas allows a broad census to be conducted of the early evolution of A stars by, for example, identifying the fraction with clear infrared excesses. A study of this kind has already been undertaken by Hales et al. (2008), who have combined IPHAS photometry with Spitzer/GLIMPSE and 2MASS data.

A work for the future is to generalise the A-star selection scheme to begin to extract a broader range of spectral types from the main stellar locus in the IPHAS colour-colour plane. In principle it is possible to map the positions of A-K near main-sequence stars as a function of reddening onto unique ( $r' - H\alpha$ ,  $r - i'$ ) values – if an effective means to distinguish and separate out higher luminosity classes can be identified. An exploration of this opportunity is now underway (Sale et al., in preparation).

## ACKNOWLEDGMENTS

We thank Kerttu Viironen who was the observer at the telescope the night the Cyg OB2 data were obtained. We also thank Jorick Vink, Danny Steeghs, Danny Lennon and Jeremy Drake for helpful comments relating to this work. The referee of this paper, Philip Massey, is thanked for his useful comments. This paper makes use of data obtained as part of the INT Photometric  $H\alpha$  Survey of the Northern Galactic Plane (IPHAS) carried out at the Isaac Newton Telescope (INT). The INT is operated on the island of La Palma by the Isaac Newton Group in the Spanish Observatorio del Roque de los Muchachos of the Instituto de Astrofísica de Canarias. All IPHAS data are processed by the Cambridge Astronomical Survey Unit, at the Institute of Astronomy in Cambridge. We also acknowledge

use of data products from the Two Micron All Sky Survey (2MASS), which is a joint project of the University of Massachusetts and the Infrared Processing and Analysis Center/California Institute of Technology (funded by the USA's National Aeronautics and Space Administration and National Science Foundation). Stuart Sale is in receipt of a studentship funded by the Science & Technology Facilities Council of the United Kingdom.

## REFERENCES

- Abt H. A., Morrell N. I., 1995, ApJS, 99, 135
- Barbon A., Hassan R.M., 1996, A&AS, 115, 325
- Bragaglia A., Tosi M., 2006, AJ, 131, 1544
- Cardelli J. A., Clayton G. C., Mathis J. S., 1989, ApJ, 345, 245
- Carraro G., Geisler D., Villanova S., Frinchaboy P. M., Majewski S. R., 2007, A&A, 476, 217
- Dickel H. R., Wendker H. J., 1978, A&A, 66, 289
- Domingo A., Figueras F., 1999, A&A, 343, 446
- Downes D., Rinehart R., 1966, ApJ, 144, 937
- Drew J. E., et al, 2005, MNRAS, 362, 753
- Gonzalez-Solares E., et al, 2008, MNRAS, submitted (arXiv:0712.0384)
- Gupta A. C., Subramaniam A., Sagar R., Griffiths W. K., 2000, A&AS, 145, 365
- Halbwachs J. L., Mayor M., Udry S., Arenou F., 2003, A&A, 397, 159
- Hales A., Barlow M. J., Drew J. E., Unruh Y. C., Greimel R., 2008, ApJ, submitted
- Hanson M. M., 2003, ApJ, 597, 957
- Houk N., Swift C. M., Murray C. A., Penston M. J., Binney J. J., 1997, in Perryman M. A. C., Bernacca P. L. eds., *Hipparcos - Venice '97*, ESA SP-402, ESA Noordwijk, p279
- Howarth I. D., 1983, MNRAS, 203, 301
- Hurley J., Tout C. A., 1998, MNRAS, 300, 977
- Irwin M. J., 1985, MNRAS, 214, 575
- Irwin M.J., 1997, in *Instrumentation for Large Telescopes (Cambridge Contemporary Astrophysics)*, ed. J. M. Espinosa, Cambridge University Press, Cambridge, England, p35.
- Jaschek C., Gomez A. E., 1998, A&A, 330, 619
- Kenyon S. J., Hartmann L., 1995, ApJS, 101, 117
- Kharchenko N. V., Piskunov A. E., Röser S., Schilbach E., Scholz R. D., 2005, A&A, 438, 1163
- Knödseder J., 2000, A&A, 360, 539
- Kroupa P., 2001, MNRAS, 322, 231
- Kumar M. S. N., Davis C. J., Grave J. M. C., Ferreira B., Froebrich D., 2007, MNRAS, 374, 54
- Lynga G., 1988, ESO Conf. Workshop Proc., no 28, 379
- Massey P., 2003, ARA&A, 41, 15
- Massey P., Thompson A. B., 1991, AJ, 101, 1408
- McCuskey S. W., Houk N., 1971 AJ, 76, 1117
- McCuskey S. W., Lee S. G., 1976 AJ, 81, 604
- Murray C. A., Penston M. J., Binney J. J., Houk N., 1997, in Perryman M. A. C., Bernacca P. L. eds., *Hipparcos - Venice '97*, ESA SP-402, ESA Noordwijk, p485
- Palla F., Randich S., Flaccomio E., Pallavicini R., 2005, ApJL, 626, 49
- alla F., Stahler S. W., 1993, 418, 414
- Pickles A. J., 1998, PASP, 110, 863 (P98)
- Piskunov A. E., Belikov A. N., Kharchenko, Sagar R., Subramaniam A., 2004, MNRAS, 349, 1449
- Reddish V. C., Lawrence L. C., Pratt N. M., 1967, PROE, 5, 112
- Sagar R., Griffiths W. K., 1991, MNRAS, 250, 683
- Schaller G., Schaerer D., Meynet G., Maeder A., 1992, A&AS, 96, 269

- Schneider N, Bontemps S., Simon R., Jakob H., Motte F., Miller M., Kramer C., Stutzki J., 2006, A&A, 2006, 458, 855
- Schlegel D. J., Finkbeiner D. P., Davis M., 1998 ApJ, 500, 525
- Siess L. Dufour E., Forestini M., 2000, A&A, 358, 593
- Valdes F., Gupta R, Rose J. A., Singh H. P., Bell D. J., 2004 ApJS, 152, 251
- Walborn N. R., Howarth I. D., Lennon D. J., Massey P., Oey M. S., Moffat A. J., Skalkowski G., Morrell N. I., Drissent L., Parker J. W., 2002, AJ, 123, 2754